68-32484

DKF

RE-ENTRY SYSTEMS DEPARTMENT

Philadelphia, Pa.

GPO PRICE $ _____

CFSTI PRICE(S) $ _____

Hard copy (HC) _____

Microfiche (MF) _____

ff 653 July 65

DRIVE — Do IT Right Initially For Value and Effectiveness

RE-ENTRY SYSTEMS DEPARTMENT — GENERAL ELECTRIC

ZERO DEFECTS

FACILITY FORM 602

N 68-33084 (ACCESSION NUMBER) (THRU)

51 (PAGES) (CODE)

CR-96375 (NASA CR OR TMX OR AD NUMBER) 12 (CATEGORY)

GENERAL ELECTRIC

JPL Contract No. 951647-Supplement
5 January 1968

FLOW FIELD COMPUTATIONS FOR BLUNT BODIES IN PLANETARY ENVIRONMENTS (EQUILIBRIUM)

Modification No. 1

FINAL REPORT

Prepared For

JET PROPULSION LABORATORY
CALIFORNIA INSTITUTE OF TECHNOLOGY
4800 OAK GROVE DRIVE
PASADENA, CALIFORNIA 91103

Prepared By

P. Hsueh

This work was performed for the Jet Propulsion Laboratory, California Institute of Technology, sponsored by the National Aeronautics and Space Administration under Contract NAS7-100.

GENERAL ELECTRIC

RE-ENTRY SYSTEMS

P. O. Box 8555 • Philadelphia, Penna. 19101

TABLE OF CONTENTS

LIST OF ILLUSTRATIONS

SUMMARY

Inviscid static and dynamic stability parameters are obtained for a family of blunted 45 degree half angle cones at Mach 10 for both ideal gas and equilibrium air flows. The results are obtained by utilization of the General Electric Flow Field Computer Programs which use appropriate numerical methods to determine both steady and unsteady inviscid flow fields. The following numerical results are obtained:

a. Dynamic stability coefficient, $C_{M_q} + C_{M_{\dot{\alpha}}}$, as a function of R_N/R_B and x_{cg}.

b. Static stability coefficient, C_{M_α}, as a function of R_N/R_B and x_{cg}.

c. Normal force coefficient slope, C_{N_α}, as a function of R_N/R_B.

d. Normal force coefficient, $C_{N_q} + C_{N_{\dot{\alpha}}}$, as a function of R_N/R_B and x_{cg}.

e. Axial force coefficient at zero angle of attack, $(C_A)_{\alpha = 0}$, as a function of R_N/R_B.

f. Ratio of center of pressure location to cone base diameter, x_{cp}/d, as a function of R_N/R_B.

g. Bow shock wave shape and position.

h. $(1/P_{t_2})\, P_\alpha = 1/P_{t_2}\, (\partial P/\partial\alpha)_{\alpha = 0}$ as a function of s/R_N for $\phi = 0^o$, 30^o, 60^o, 90^o, where P_{t_2} is model stagnation pressure, P is model surface pressure, ϕ is azimuthal angle and s is distance measured along model surface from forward point on the axis of symmetry.

i. Cone surface pressure, (P/P_{t_2}), as a function of s/R_N.

For the real gas case, the shock layer flow downstream of the sonic line on the sphere is everywhere supersonic, and no difficulty was encountered in the computations.

For the ideal gas case, there exists a subsonic layer near the conical part of the body surface where the flow is otherwise generally supersonic. The approximation made in Section 3 enabled the completion of the computation for this case. The effect of the approximation is found to be significant for bodies of large bluntness ratios but is negligible for bodies of small bluntness ratios.

NOMENCLATURE

a, b = γ coefficients

A = cone reference area, $\pi d^2/4$, ft^2

C_A = axial force coefficient, $\dfrac{\text{axial force}}{q_\infty A}$

C_M = pitching moment coefficient,

$$= \frac{\text{moment about cone center of rotation } (x_{cg})}{q_\infty Ad}$$

C_{M_α} = $\partial C_m/\partial\alpha$ per radian

$C_{m_q} + C_{m_{\dot\alpha}} = \partial C_m/\partial(\frac{qd}{u_\infty}) + \partial C_m/\partial(\dot\alpha d/u_\infty)$ per radian

C_N = normal force coefficient, $\dfrac{\text{normal force}}{q_\infty A}$

C_{N_α} = $\partial C_N/\partial\alpha$, per radian

$C_{N_q} + C_{N_{\dot\alpha}} = \dfrac{u_\infty}{d}\dfrac{\partial C_N}{\partial q} + \dfrac{\partial C_N}{\partial\alpha}$, per radian

C_o Speed of sound, $(\frac{\partial p}{\partial\rho})_s$

$\frac{D}{Dt}$ Material derivative

d Base diameter, ft

$d\ell$ Differential distance along Mach lines

e_o^2 $\left(\dfrac{\partial P}{\partial S}\right)_p$

F_N Normal force

h Enthalpy

L Reference length, body length, ft

M Mach number

n Order of derivative of angle of attack or pitch velocity being considered

$\vec{n}$ Unit inward vector normal to the surface indicated by its subscript

P Pressure, lb/ft^2

P_{t_2} Model stagnation pressure, lb/ft^2

q	Pitch rate
q_∞	Free stream dynamic pressure
R	Gas constant
R_B	Radius of cone base
R_N	Radius of cone nose
s	Distance measured along surface from forward point (nose tip) on s axis of symmetry
S	Entropy
t	Time
T	Temperature
u, v, w	Components of $\vec{V}$ in the x, r, and φ directions
V	Magnitude of velocity in meridional plane
$\vec{V}$	Fluid velocity relative to the body fixed coordinate system
x, r, φ	Coordinate directions
$\vec{x}, \vec{r}, \vec{\varphi}$	Unit vectors in the coordinate directions
x, y, z	Coordinate directions
x_o	Distance from x, y, z origin to center of spherical nose
$\vec{x}, \vec{y}, \vec{z}$	Unit vectors in the coordinate directions
Z	Compressibility factor
α	Angle of attack
γ	Ideal gas ratio of specific heats
γ^*	$\frac{\rho C_o^2}{P} = \frac{\rho}{P}\left(\frac{\partial P}{\partial \rho}\right)_S$
∇	Gradient operator
δ	An indicator which is defined to be $\delta = 1$ for the axisymmetric case and $\delta = 0$ for the two-dimensional case
θ	Flow direction

μ	Mach angle
ρ	Density
ψ	Stream function
$\vec{\Omega}$	Angular velocity of the body
σ	Shock angle

Subscripts

B	Body surface
cg	Center of gravity (center of rotation)
j	This subscript indicates whether the perturbation is caused by angle of attack (j = 1) or pitch rate (j = 2)
n	This subscript indicates the order of derivative of angle of attack or pitch velocity being considered
N	Normal to shock, nose
0	Zero yaw
S	Isentropic process
s	Immediately downstream of shock wave
∞	Free stream
1	Perturbations due to α and its derivatives
2	Perturbations due to q and its derivatives

SECTION 1
INTRODUCTION

The work reported herein was performed by the General Electric Company Re-entry Systems Department, Philadelphia, Pa., under Jet Propulsion Laboratory Contract No. 951647 - supplement. The author wishes to acknowledge Mr. Charles Kyriss for his active interest and many valuable suggestions, and Mr. P. C. Townsend for preparing the tables and graphs.

1.1 STUDY OBJECTIVE

The objective of this study is to determine the static and dynamic stability parameters for a family of blunted 45 degree half angle cone bodies at two free stream conditions.

1.2 STUDY CONFIGURATIONS AND FREE STREAM CONDITIONS

The configurations being considered are 45 degree half angle sphere-cones with nose-to-base radius ratios (R_N/R_B) of 0, 0.25, 0.50, 0.75, and 1.00. (See Figure 1-1.) The two free stream conditions are as follows:

a. Ideal gas ($\gamma = 1.4$)

   Base diameter = 5.5 inches

   $M_\infty = 10$

   $u_\infty = 4080$ ft/sec

   $\rho_\infty = 2.68 \times 10^{-4}$ lb_m/ft^3

   $P_\infty = 4.65 \times 10^{-4}$ atmosphere

b. Real gas (air in chemical equilibrium)

   Base diameter = 2.0 inches

   $u_\infty = 10820$ ft/sec

$\rho_\infty = 0.74713 \times 10^{-4}$ lb_m/ft^3

$P_\infty = 0.91764 \times 10^{-4}$ atmosphere

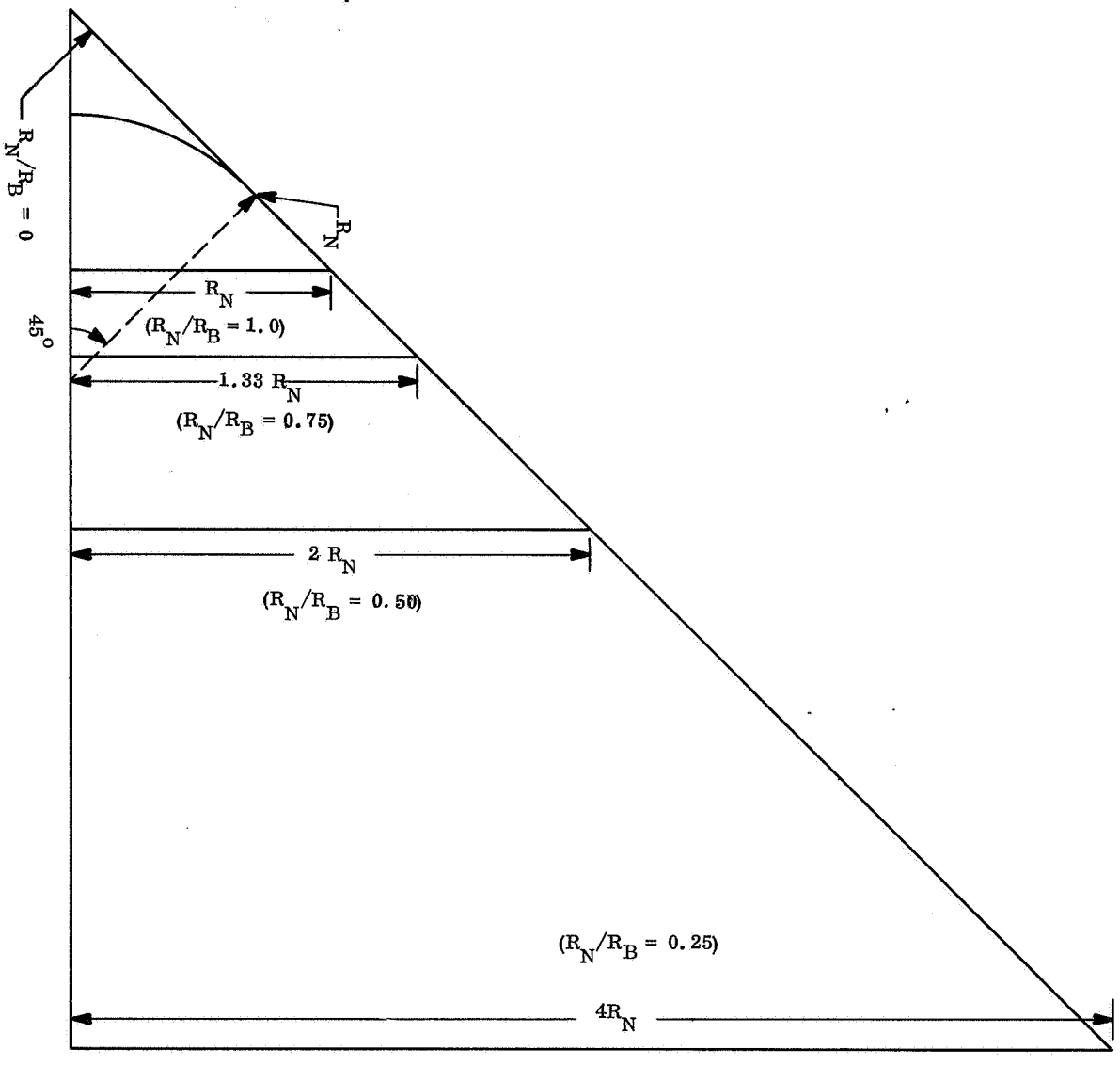

Figure 1-1. Study Configurations

The coordinate system used in this report is shown in Figure 1-2.

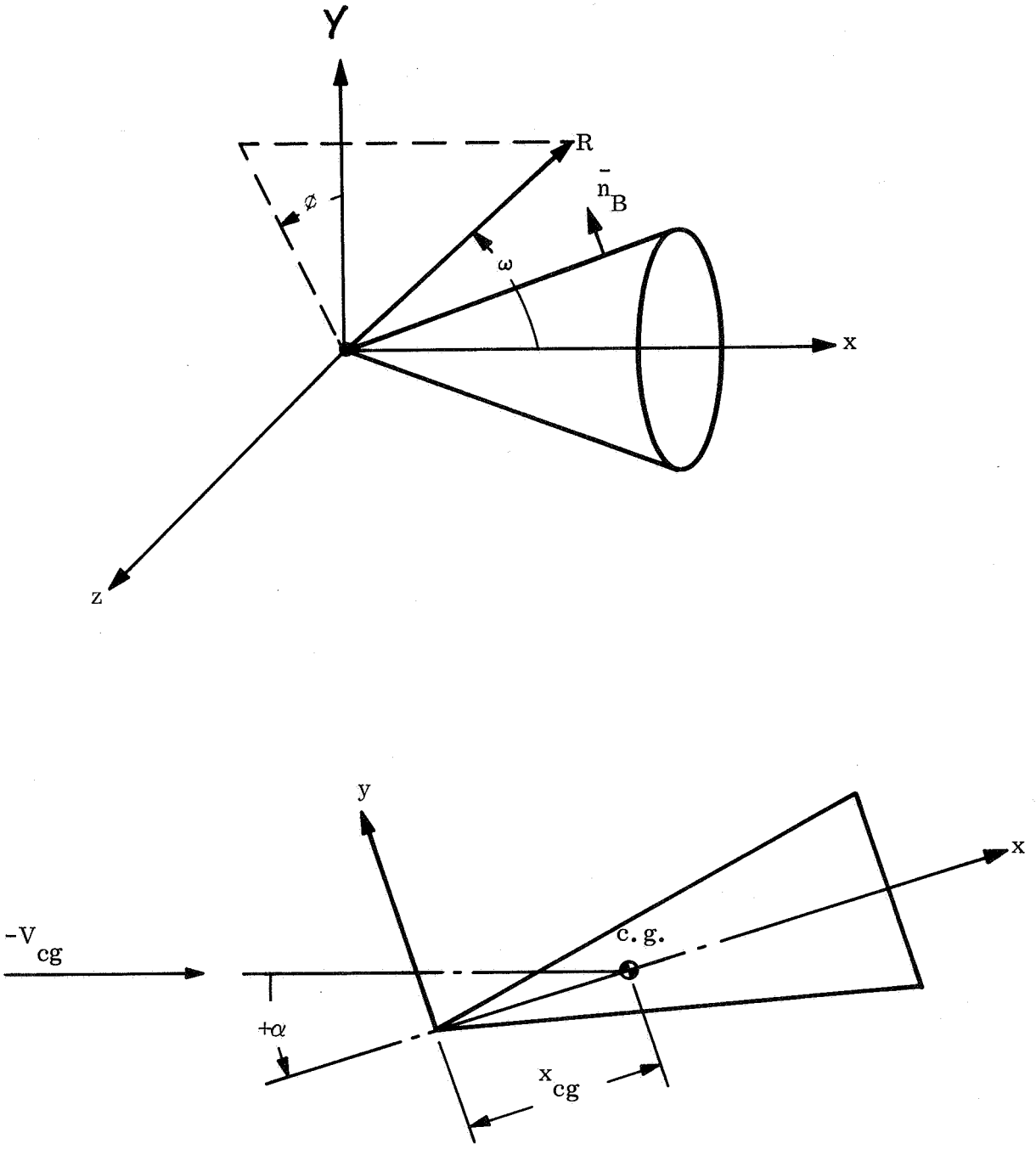

Figure 1-2. The Spherical Coordinates System and the Angle-of-Attack

SECTION 2

TECHNICAL APPROACH

The methods used in this report are analytical in nature. Mathematical models are constructed to represent both steady and unsteady state flow fields. The governing equations and boundary conditions are solved by computer, using appropriate numerical methods. In this section, the equations and boundary conditions as well as the assumptions for both steady and unsteady state flow conditions will be discussed briefly. References are given for more detailed descriptions.

2.1 THE ZERO YAW STEADY STATE SOLUTION

The purpose of this analysis is to generate the drag coefficients and to pave the way for the unsteady part of the problem. The solution is obtained by means of the GE Flow Field Program which is capable of both real and ideal gas computations in shock layers surrounding a variety of axisymmetric and two-dimensional bodies. It is a numerical solution of the laws of conservation of mass, momentum, and energy. (Here the viscous effect is not considered and adiabatic flow is assumed):

$$\nabla \cdot (\rho \vec{V}) = 0 \tag{2-1}$$

$$\vec{V} \cdot \nabla \vec{V} + \frac{1}{\rho} \nabla p = 0 \tag{2-2}$$

$$\vec{V} \cdot \nabla S = 0 \tag{2-3}$$

and the state relations:

$$\frac{P}{\rho} = ZRT \tag{2-4}$$

$$S = S(\rho, T) \tag{2-5}$$

$$Z = Z(\rho, T),\ Z = (\rho, S) \tag{2-6}$$

$$P = P(\rho, S) \tag{2-7}$$

and

$$h = h(\rho, S) \tag{2-8}$$

The last five of these relations are in tabular form, for air treated as a real gas in chemical equilibrium.

The GE solution also uses a parameter γ^* (Reference 1), where γ^* is defined as:

$$\gamma^* = \frac{\rho}{P}\left(\frac{\partial P}{\partial \rho}\right)_S \tag{2-9}$$

and is computed as a function of S and p, using the expression:

$$\gamma^* = \frac{a}{P} + b \tag{2-10}$$

The coefficients a and b are tabulated as functions of entropy and pressure. All thermodynamic properties were originally taken from References 2, 3, 4. Tables were reorganized and stored on computer tape by Stamm (Reference 5) and Edsall (Reference 6). Empirical fits and table interpolation schemes are accurate to within 1 percent of the data being represented.

If an ideal gas calculation is desired, Z becomes unity, γ^* becomes the ratio of specific heats*, and the real gas relations (Equations 2-3, 2-7, and 2-8) are reduced to several ideal gas relations:

*For an ideal gas a = 0 and b = the ratio of specific heats

$$P \rho^{-\gamma} = \text{constant along streamlines} \tag{2-11}$$

$$\frac{1}{2} V^2 + \frac{\gamma}{\gamma - 1} \frac{P}{\rho} = \text{constant} \tag{2-12}$$

The boundary conditions imposed on the problem consist of the free stream conditions upstream of the shock wave*, and the condition that no mass flows through the body surface. Since the mathematical character of the governing equations is different on opposite sides of the sonic line, the solution is carried out in a different way in the transonic and supersonic regions of the shock layer. The solution in both regions is carried out on a GE 635 computer.

2.2 THE TRANSONIC REGION

The computation for a blunt body is started in the transonic region, which includes the sonic line and a small part of the shock layer on each side of the sonic line. A coordinate grid of streamlines and the lines normal to them is used. The solution is a direct one (Reference 1). It is started by making an initial estimate of the shock shape and of the pressure distribution at the body surface. The location of a streamline a small distance from this body is then computed (as well as the value of the flow field variables on it) to satisfy the governing equations. This process of stepping to the next streamline is repeated until a new shock wave, which satisfies the conservation of mass law, is reached. The shape of this new shock wave, as well as the pressures just downstream of it, are compared with the shape and corresponding pressures for the initial estimate. New estimates of shock shape and body pressure distribution are based on this comparison and on a general inspection of the results obtained in the entire transonic region. This iterative cycle is repeated until the estimates and computed values agree closely. It is usually possible to obtain pressure downstream of the estimated and computed shock waves to agree within 3 percent, and to get the estimated and computed shock waves to coincide within 0.004 of the body radius of curvature at the stagnation point. At each step of the iteration, the choice of a new estimate

*Applied through the Rankine-Hugoniot relations

of shock shape and body pressure distribution is made by the operator; all other iterative cycles are automatic. Detailed discussion and a guide to converging the zero yaw transonic solution is given in Reference 7.

2.3 THE POINTED CONE SOLUTION

When a flow field solution is needed for a pointed body, the supersonic program provides it. However, the supersonic program requires a solution along a starting line. This starting solution is obtained by approximating a small portion of the nose of the pointed body by a pointed cone. The solution for a pointed cone is then obtained by the method of Taylor and Maccoll (Reference 8), modified to provide a real gas solution, if desired. This solution has been included in a single computer program with the unsteady solution for the pointed cone. A detailed derivation of this solution appears in References 9 and 10.

2.4 THE SUPERSONIC REGION

The steady-state solution in the supersonic region is carried out by the method of characteristics for both pointed and blunt bodies. Three basic directions are used: the flow direction (constant ψ, constant S) and the directions of the Mach lines. The angles between the Mach lines and the flow direction are:

$$\pm\mu = \sin^{-1}\left(\frac{1}{M}\right) \tag{2-13}$$

The Mach lines are the characteristics (in the mathematical sense) of the continuity and momentum equations. Changes along these lines are defined by:

$$\frac{d\theta}{d\ell} \pm \frac{\delta}{r} \sin\mu \sin\theta \pm \frac{\cot}{\rho V^2} \frac{dP}{d\ell} = 0 \tag{2-14}$$

where

θ = the flow angle measured from the axial.

ℓ = the distance measured along a characteristic.

The + and - signs apply to the left and right Mach lines, respectively.

In addition to Equation (2-14), the equation of state, the condition of constant total energy, and the condition of isentropic flow along streamlines must be satisfied. The numerical solution is started from a line along which the solution has previously been computed by either the transonic or pointed cone program. References 1 and 11 give detailed discussions.

2.5 THE UNSTEADY FLOW FIELD SOLUTIONS

To obtain both the static and dynamic stability parameters, the unsteady flow field must be analyzed. In this analysis, the equations and boundary conditions are described in body fixed coordinates. The equations become

$$\frac{\partial \rho}{\partial t} + \nabla \cdot (\rho \vec{V}) = 0 \tag{2-15}$$

$$\frac{\partial \vec{V}}{\partial t} + (\vec{V} \cdot \nabla) \vec{V} + \frac{\nabla P}{\rho} = -\frac{d \vec{V}_{cg}}{dt} - \vec{\Omega} \times \vec{V}_{cg} + \vec{r} \times \frac{d \vec{\Omega}}{dt}$$

$$+ (\vec{\Omega} \times \vec{r}) \times \vec{\Omega} - 2 (\vec{\Omega} \times \vec{V}) \tag{2-16}$$

$$\frac{DS}{Dt} = 0 \tag{2-17}$$

where $\vec{V}_{cg}$ (t) is the linear velocity of the center of gravity and $\vec{\Omega}$ (t) is the rotational velocity.

The thermodynamic state relations are the same as Equations (2-4) to (2-10).

The boundary condition on the body surface is that the normal component of the velocity vector is zero, i. e.

$$\vec{V} \cdot \vec{n}_B = 0 \tag{2-18}$$

The boundary conditions downstream of the shock are obtained through Rankine-Hugoniot relations.

Since the steady state solution of the problem has been obtained in the previous sections, the unsteady effects are evaluated by the method of small perturbation. To do so, the flow field parameters are expressed by the sum of the value it has in the zero yaw steady state case plus contributions proportional to angle of attack α, pitch rate q, and their time derivatives. Using pressure P as an example:

$$P = P_o + \left[P_{10}\,\alpha + P_{11}\left(\frac{L}{u_\infty}\right)\dot{\alpha} + P_{12}\left(\frac{L}{u_\infty}\right)^2 \ddot{\alpha} + \ldots \right.$$

$$\left. + \left(P_{20} - P_{10}\,\frac{x_{cg}}{L}\right)\left(\frac{L}{u_\infty}\right) q + \ldots \right] \cos\phi \tag{2-19}$$

where

x_{cg} = location of center of gravity

L = reference length

u_∞ = free stream velocity

ϕ = meridional angle.

Substitution of this equation (and similar expressions for the remaining flow field variables) into the governing equations (2-1) to (2-4), yields:

$$\left.\begin{aligned}
&\frac{\partial \rho_j}{\partial t} + \nabla \cdot (\rho_o \vec{V}_j + \rho_j \vec{V}_o) = 0; \\
&\frac{\partial \vec{V}_j}{\partial t} + (\vec{V}_o \cdot \nabla)\vec{V}_j + (\vec{V}_j \cdot \nabla)\vec{V}_o + \frac{\nabla P_j}{\rho_o} - \frac{\nabla P_o}{\rho_o^2}\rho_j = \vec{F}_j; \\
&\frac{\partial S_j}{\partial t} + \vec{V}_o \cdot \nabla S_j + \vec{V}_j \cdot \nabla S_o = 0 \\
&P_j = C_o^2 \rho_j + e_o^2 S_j;
\end{aligned}\right\} \quad j=1,2 \qquad (2\text{-}20)$$

where

C_o = speed of sound and $e_o^2 = (\partial P/\partial S)_\rho$

$$\vec{F}_j = \begin{cases} -u_\infty \dfrac{d\bar{\alpha}}{dt}\vec{y}, & j = 1 \\ 2(\vec{V}_o \times \vec{z})\bar{q}\dfrac{u_\infty}{L} + \dfrac{u_\infty^2}{L}\bar{q}\vec{y} + (\vec{r} \times \vec{z})\dfrac{u_\infty}{L}\dfrac{d\bar{q}}{dt}, & j = 2 \end{cases}$$

The effect of the unsteady motion of the body on the flow field variables is obtained through a numerical solution of these equations. The static and dynamic stability coefficients are obtained by integrating the appropriate pressure derivatives ($P_{10} = \partial P/\partial \alpha$, etc.) over the body surface. Detailed discussion can be found in References 7 and 12.

SECTION 3
DIFFICULTY ENCOUNTERED

During the course of computation, one difficulty was encountered. For the case of a blunted cone, the transonic flow field as described in Section 2.2 was calculated first. For both the ideal and the real gas, the supersonic flow started on the spherical portion of the body. The calculation was then carried on by the supersonic program as discussed in Section 2.4. However when the flow reached the conical portion of the body, the flow was being compressed slightly, whereas on the spherical portion, the fluid was being expanded. The Mach number decreased slightly and then approached a constant value. In the real gas case, even though the Mach number decreased, the flow remained supersonic. In other words, in the real gas case, the flow remained supersonic everywhere once it became supersonic. However in the ideal gas case, when the Mach number decreased, the flow near the body became subsonic. That is, in the ideal gas case, there existed a subsonic layer near the body in the otherwise generally supersonic region. It is known that the method of characteristic discussed in Section 2.4 fails when there is subsonic flow in the region. It is noted here that this situation does not happen when one deals with vehicles of small cone angle since the compression effect is less. One might hope that a higher free stream Mach number may raise the Mach number near the body so that the flow will not become subsonic. The author has examined this phenomenon and found that it exists up to M = 20. According to Reference 13, the flow patterns remain generally the same for a certain cone shape at high Mach numbers. Therefore, it may be concluded that for a 45-degree half angle cone this phenomenon exists at all Mach numbers.

3.1 APPROXIMATION

To overcome this obstacle without significantly altering the method of calculation, it was decided to adjust the boundary condition slightly in the supersonic flow region such that the Mach number would remain greater than unity. Since the result of the transonic solution is used as the boundary condition of the supersonic calculation, an adjustment on its properties will alter the Mach number in the field. In this case, it was decided to raise the

density distribution by 3.5 percent, while keeping the rest of the properties (pressure, velocity vector,etc.), the same. The ideal gas case result presented in Section 4 was obtained by using this approximation. The error is estimated in the next section. This approximation was not needed in the real gas case.

3.2 ESTIMATED ERROR

To estimate the error generated by using the above approximation, the following calculations were performed. Since the real gas case was calculated without using this approximation, the results of this case were compared with the additional result obtained by purposely using the approximation in the real gas case. It is found that the error is significant for a short body, while very insignificant for a comparatively longer body. The following table gives the error due to this approximation with respect to the static and the dynamic stability coefficients.

Table 3-1. Estimates of Error in Ideal Gas Aerodynamic Coefficients

Coefficient	Center of Rotation	Percentage Error				
		$\frac{R_N}{R_B} = 1$	$\frac{R_N}{R_B} = 0.75$	$\frac{R_N}{R_B} = 0.5$	$\frac{R_N}{R_B} = 0.25$	$\frac{R_N}{R_B} = 0$
C_A		+6.2	+3.35	+1.87	0	0
C_{N_α}		+11	+9.9	+4.05	+1.27	0
C_{M_α}	Nose Tip	-9.1	-8.4	-1.9	-0.5	0
	Base	-6.0	-7.35	+2.17	+1.48	0
$C_{N_\alpha} + C_{N_q}$	Nose Tip	+21	+9.3	+4.88	+0.95	0
	Base	+32.8	+8.8	+5.75	+0.6	0
$C_{M_\alpha} + C_{M_q}$	Nose Tip	-20	-7.8	-4.1	-0.65	0
	Base	-34.5	-4.73	-6.75	-0.95	0

SECTION 4

NUMERICAL RESULTS

In this section, the numerical results of the computations for the two cases described in Section 1 are presented. The methods used to generate these results were discussed in Section 2. An approximation was made when a difficulty was encountered in computing the ideal gas case. The error was estimated in Section 3. Since the error was found significant for large bluntness ratio configurations, comparison between the ideal and the real gas cases will be made only for configurations of small bluntness ratios.

The dynamic stability coefficients, $C_{M_q} + C_{M_{\dot{\alpha}}}$, due to both the pitching rate and the rate of angle of attack are shown in Figures 4-1 and 4-2 as a function of bluntness ratio and the center of rotation for ideal and real gas cases, respectively. It is seen that the effects are smaller for vehicles with large bluntness ratios. For vehicles with small bluntness ratios, the coefficients are almost the same in both ideal and real gas cases.

Figures 4-3 and 4-4 show the static stability coefficients as a function of bluntness ratio and the center of rotation for both the ideal and the real gas cases, respectively.

Figures 4-5 and 4-6 show the variation of the normal force coefficient slope with respect to bluntness ratio for both cases.

The normal force coefficients for both cases as a function of bluntness ratio and the location of center of rotation are shown in Figures 4-7 and 4-8. The coefficient increases when R_N/R_B decreases.

The axial force coefficients at zero angle of attack for both cases are shown in Figures 4-9 and 4-10, respectively. It is as expected that the coefficients are higher for more blunted configurations.

Figures 4-11 and 4-12 show the center of pressure location with respect to bluntness ratio.

The values of $(1/P_{t_2})(\partial P/\partial \alpha)_{\alpha = 0}$, as a function of s/R_N and the azimuthal angle ϕ for both cases are shown in Figures 4-13 and 4-14.

The shock shape and the body configurations are shown in Figures 4-15 and 4-16 for both cases.

Finally, the pressure distributions for both cases are shown in Figures 4-17 and 4-18. The pressures at the end of the small bluntness vehicles approach those of the pointed cone shape.

Numerical results in tabular form are given in Appendix A.

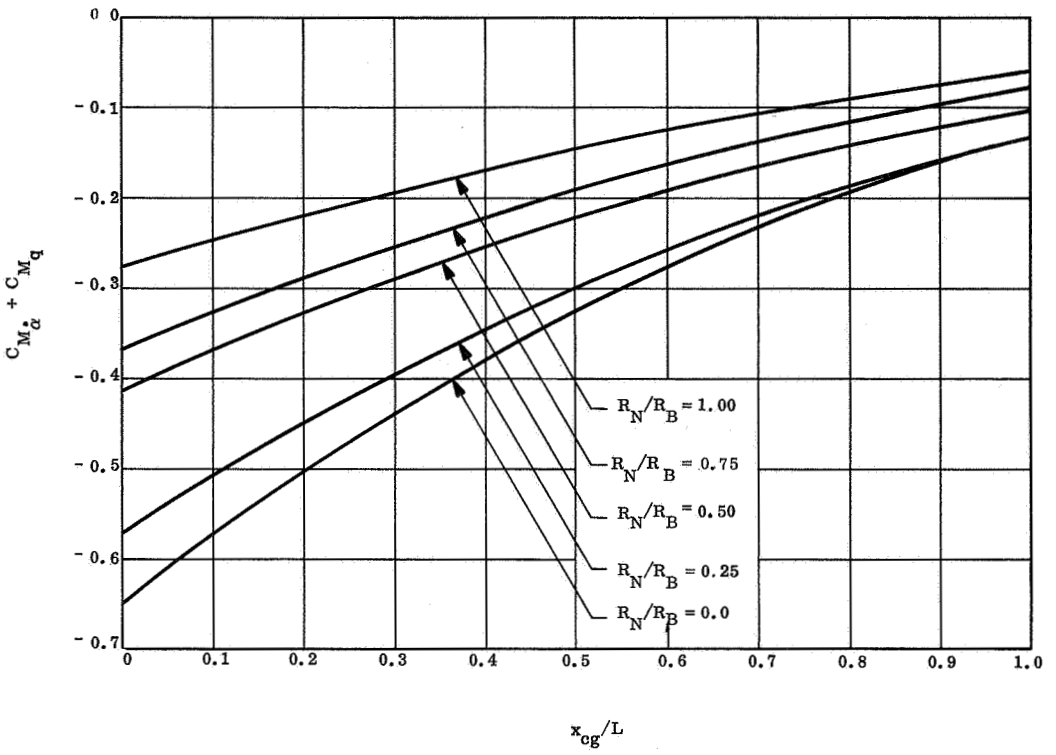

Figure 4-1. Dynamic Stability Coefficient, $C_{M_q} + C_{M_{\dot{\alpha}}}$, as a Function of R_N/R_B and x_{cg} for Ideal Gas Case

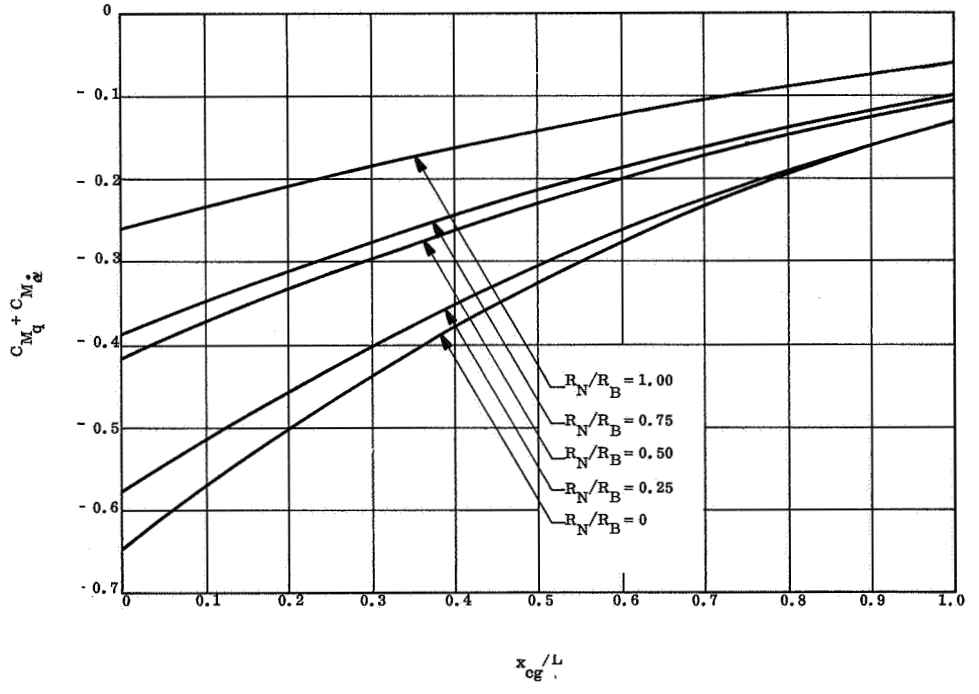

Figure 4-2. Dynamic Stability Coefficient, $C_{M_q} + C_{M_{\dot{\alpha}}}$, as a Function of R_N/R_B and x_{cg} for Real Gas Case

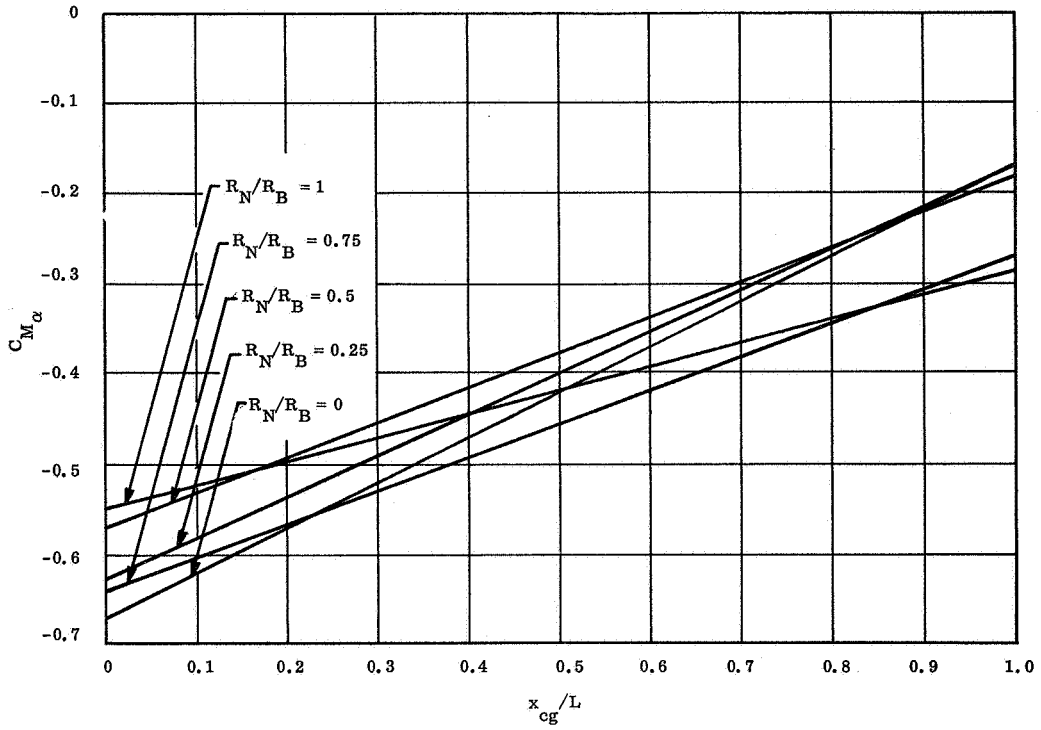

Figure 4-3. Static Stability Coefficient, C_{M_α}, as a Function of R_N/R_B and x_{cg} for Ideal Gas Case

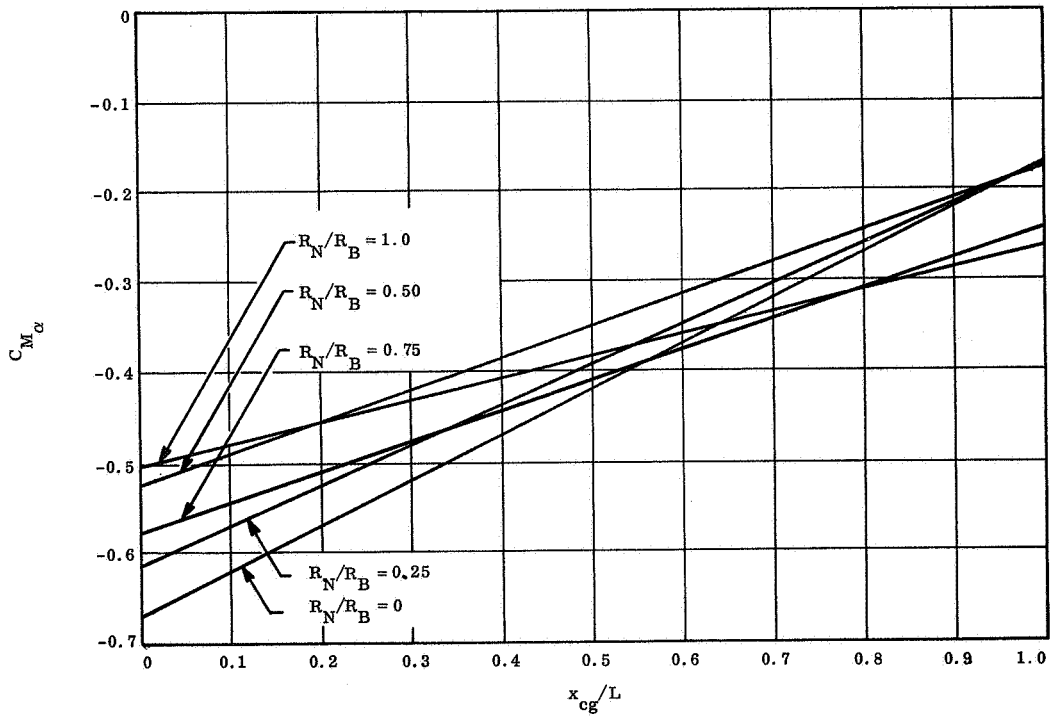

Figure 4-4. Static Stability Coefficient, C_{M_α}, as a Function of R_N/R_B and x_{cg} for Real Gas Case

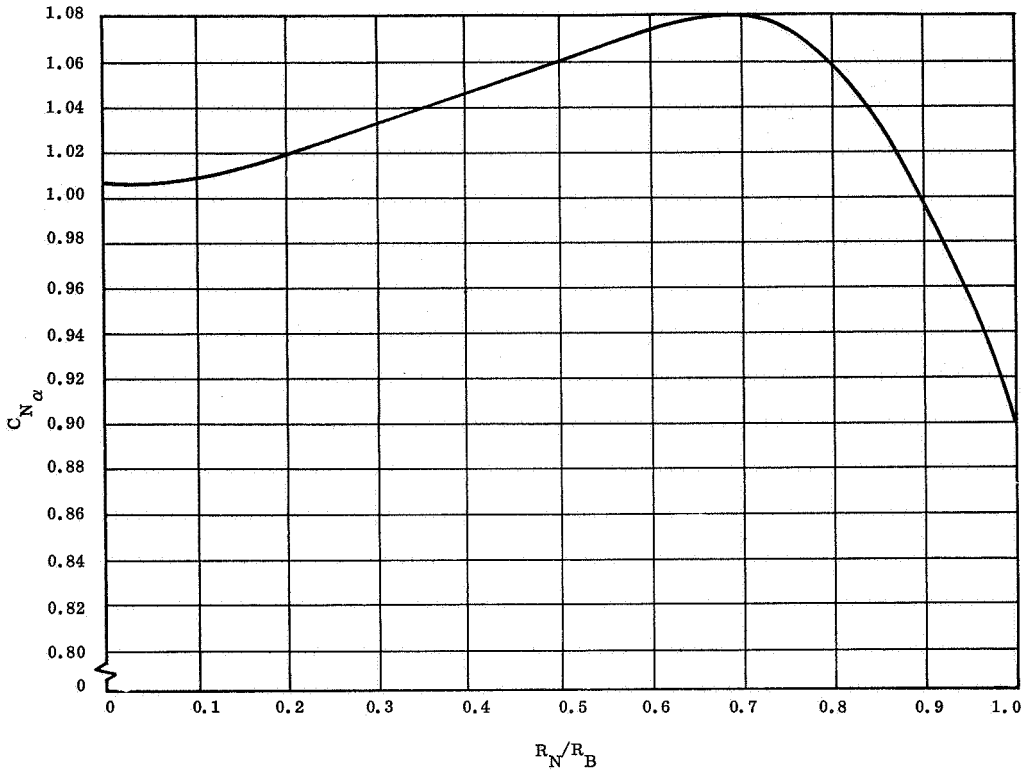

Figure 4-5. Normal Force Coefficient Slope, C_{N_α}, as a Function of R_N/R_B for Ideal Gas Case

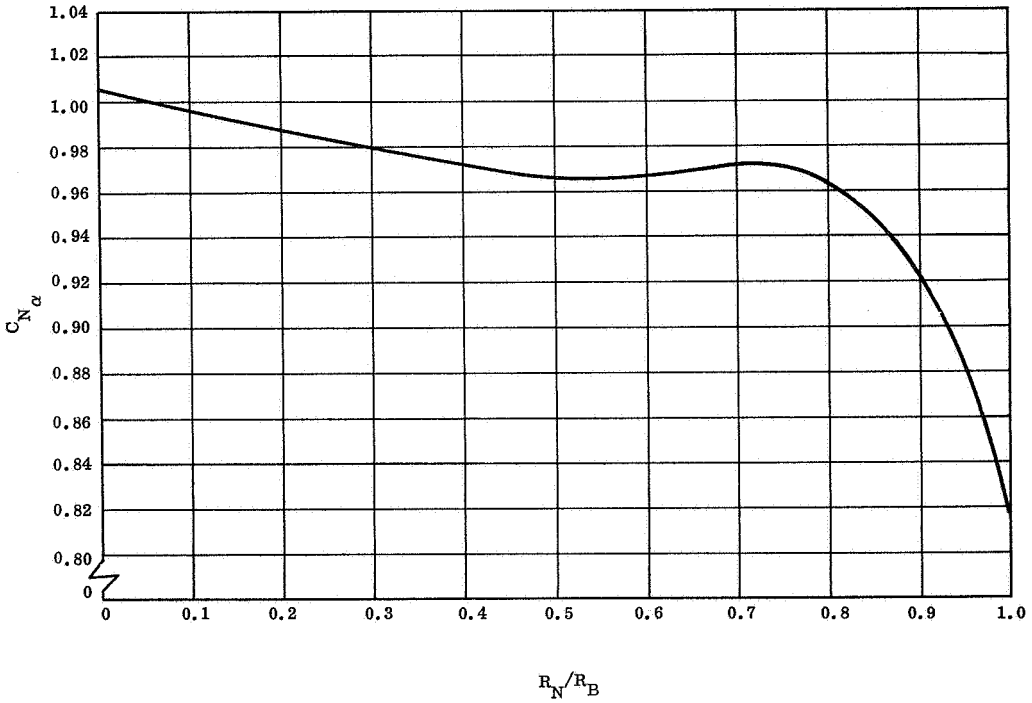

Figure 4-6. Normal Force Coefficient Slope, C_{N_α}, as a Function of R_N/R_B for Real Gas Case

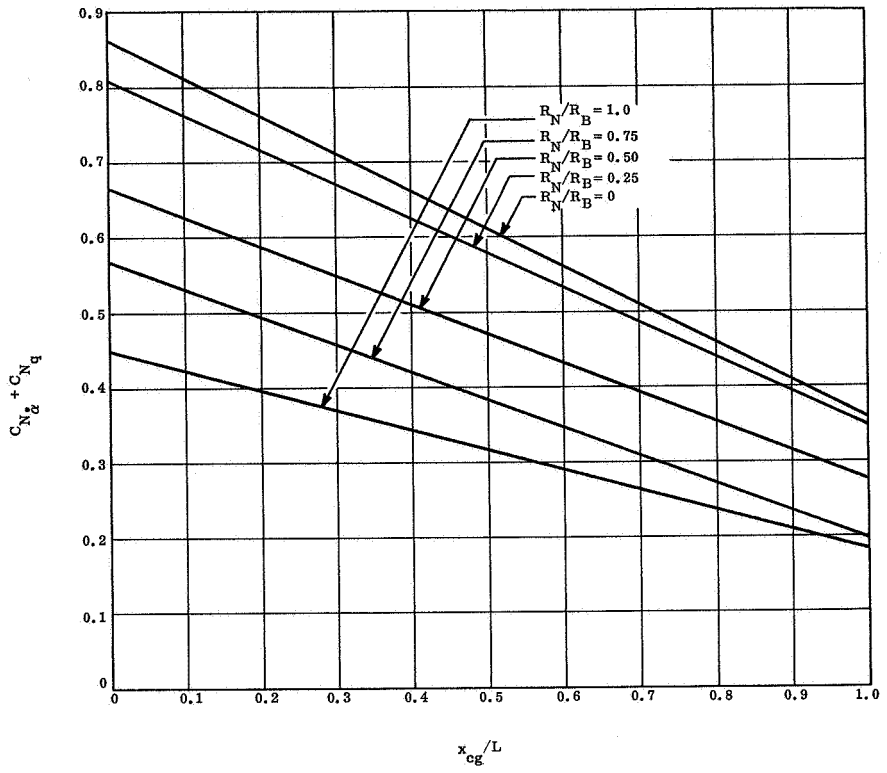

Figure 4-7. Normal Force Coefficient, $C_{N_{\dot{\alpha}}} + C_{N_q}$, as a Function of R_N/R_B and x_{cg} for Ideal Gase Case

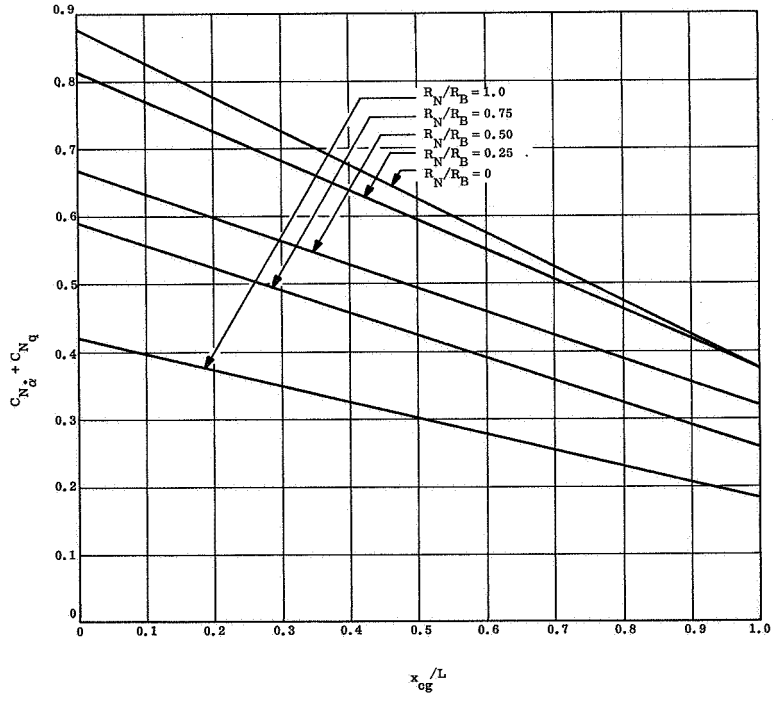

Figure 4-8. Normal Force Coefficient, $C_{N_{\dot{\alpha}}} + C_{N_q}$, as a Function of R_N/R_B and x_{cg} for Real Gas Case

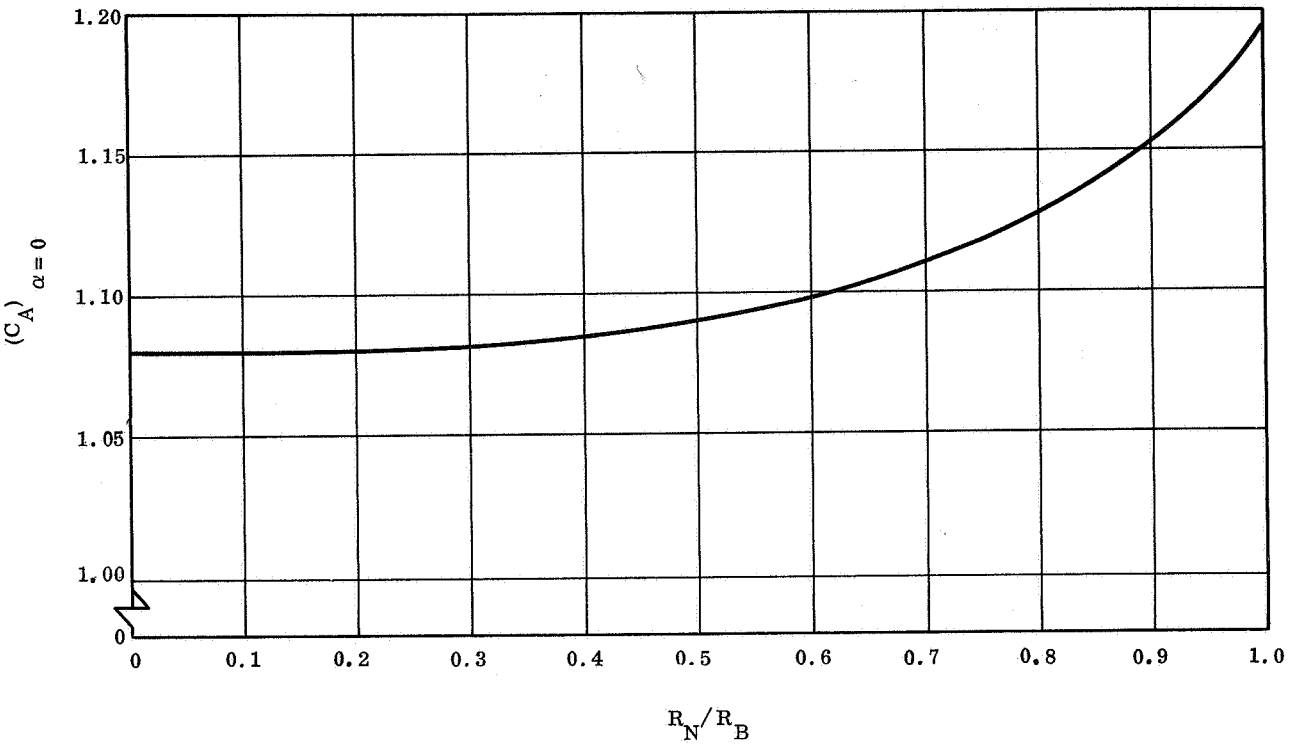

Figure 4-9. Axial Force Coefficient at Zero Angle of Attack, $(C_A)_{\alpha = 0}$, as a Function of R_N/R_B for Ideal Gase Case

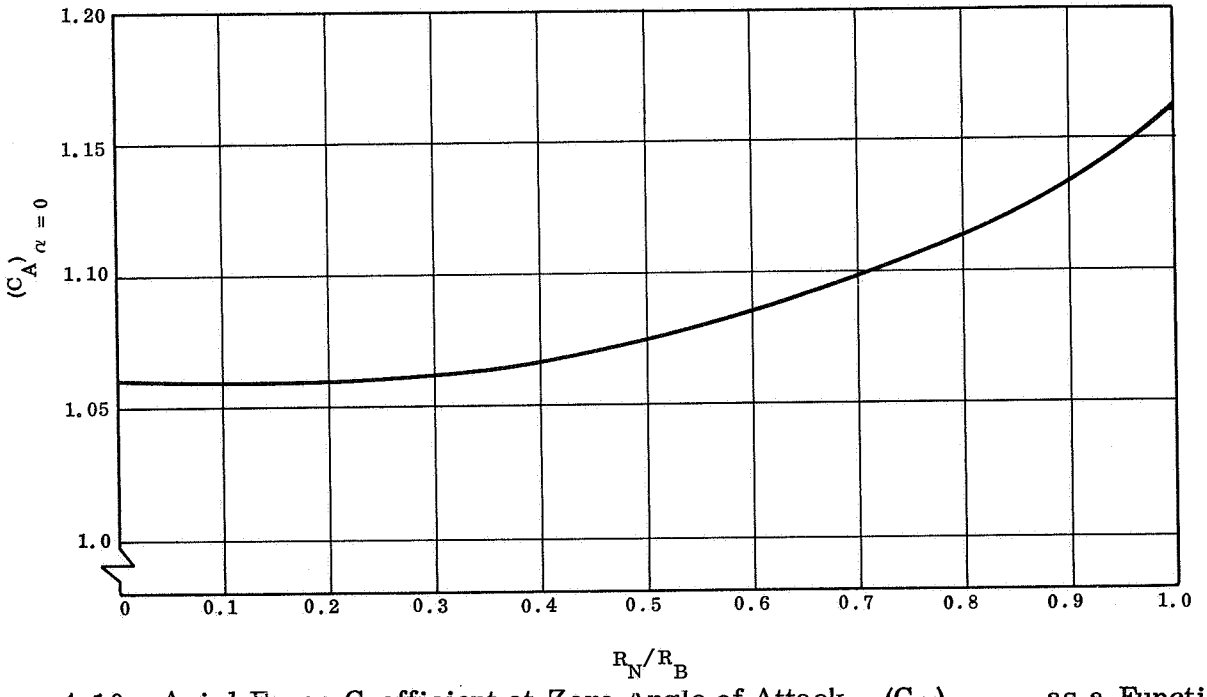

Figure 4-10. Axial Force Coefficient at Zero Angle of Attack , $(C_A)_{\alpha = 0}$, as a Function for R_N/R_B for Real Gas Case

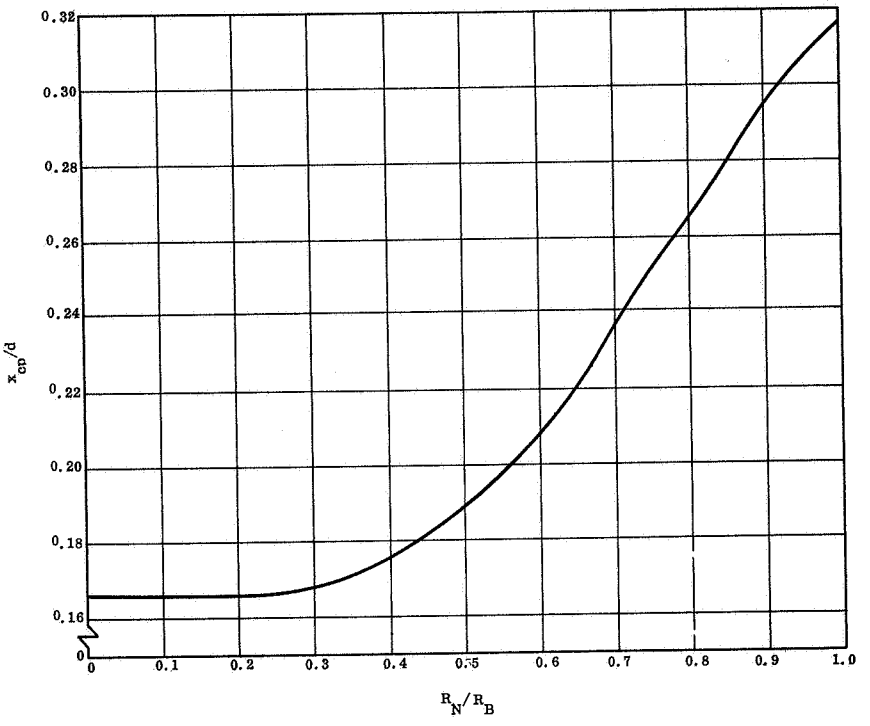

Figure 4-11. Ratio of Center of Pressure Location to Cone Base Diameter, x_{cp}/d, as a Function of R_N/R_B for Ideal Gas Case

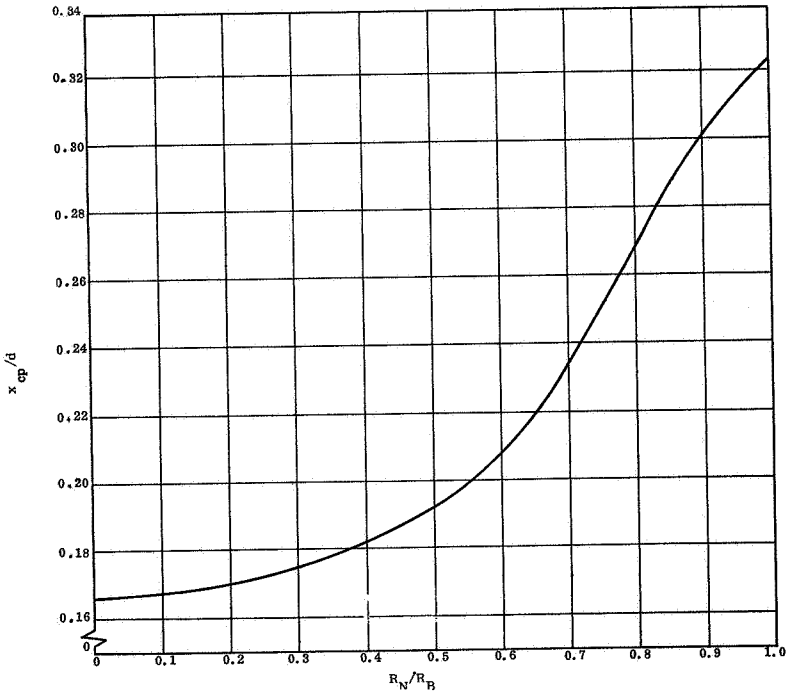

Figure 4-12. Ratio of Center of Pressure Location to Cone Base Diameter, x_{cp}/d, as a Function of R_N/R_B for Real Gas Case

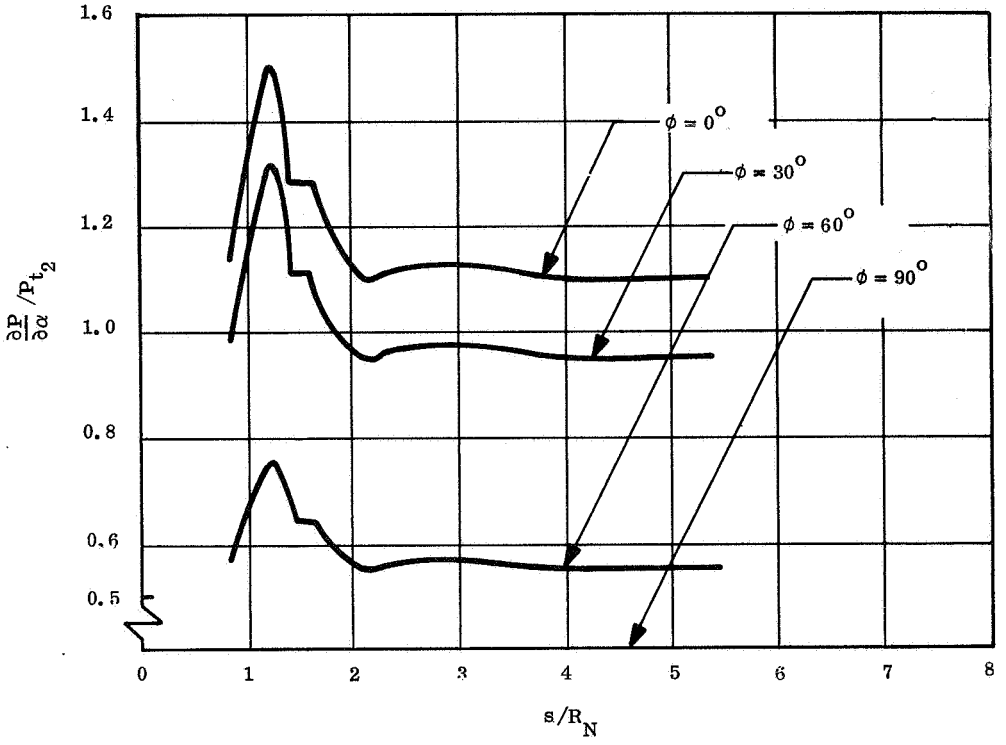

Figure 4-13. The Value of $(1/P_{t_2})\ (\partial P/\partial \alpha)_{\alpha = 0}$, as a Function of s/R_N and the Azimuthal Angle ϕ for Ideal Gas Case

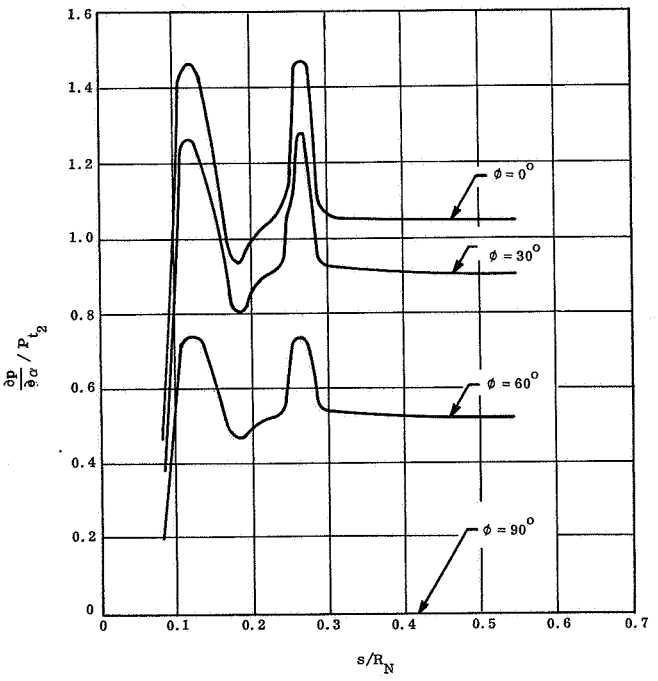

Figure 4-14. The Value of $(1/P_{t_2})\ (\partial\ P/\partial\ \alpha)_{\alpha = 0}$, as a Function of s/R_N and the Azimuthal Angle ϕ for Real Gas Case

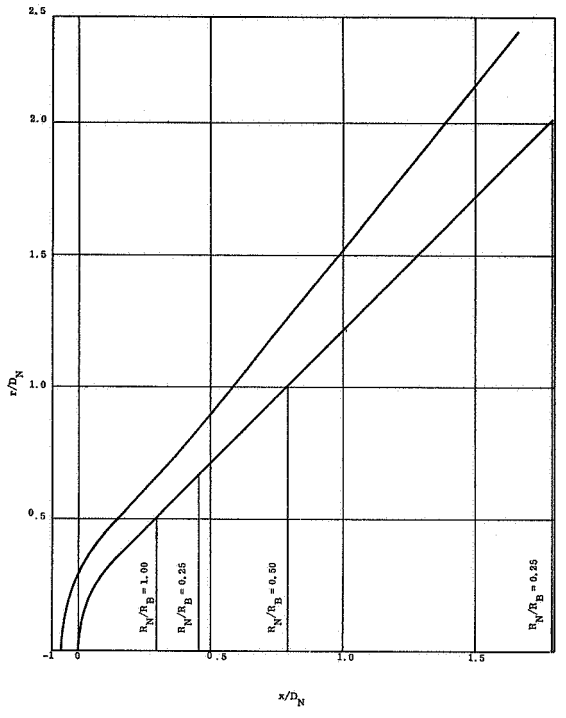

Figure 4-15. Bow Shock Wave Shape and Position for Ideal Gas Case

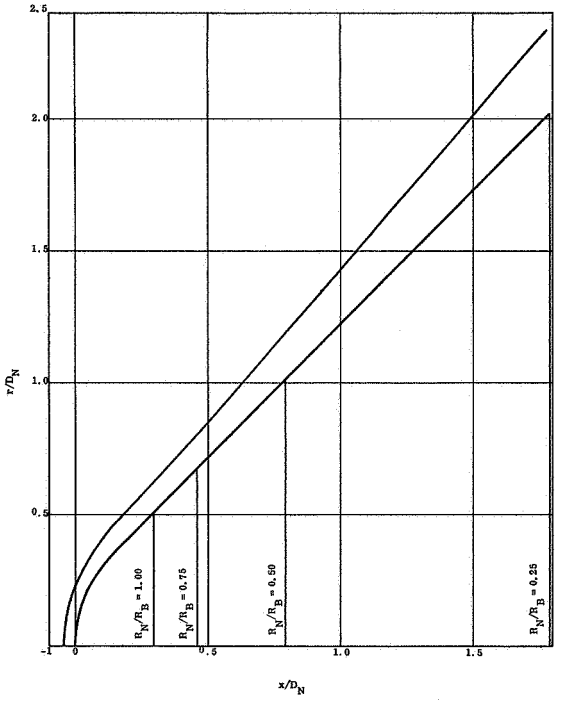

Figure 4-16. Bow Shock Wave Shape and Position for Real Gas Case

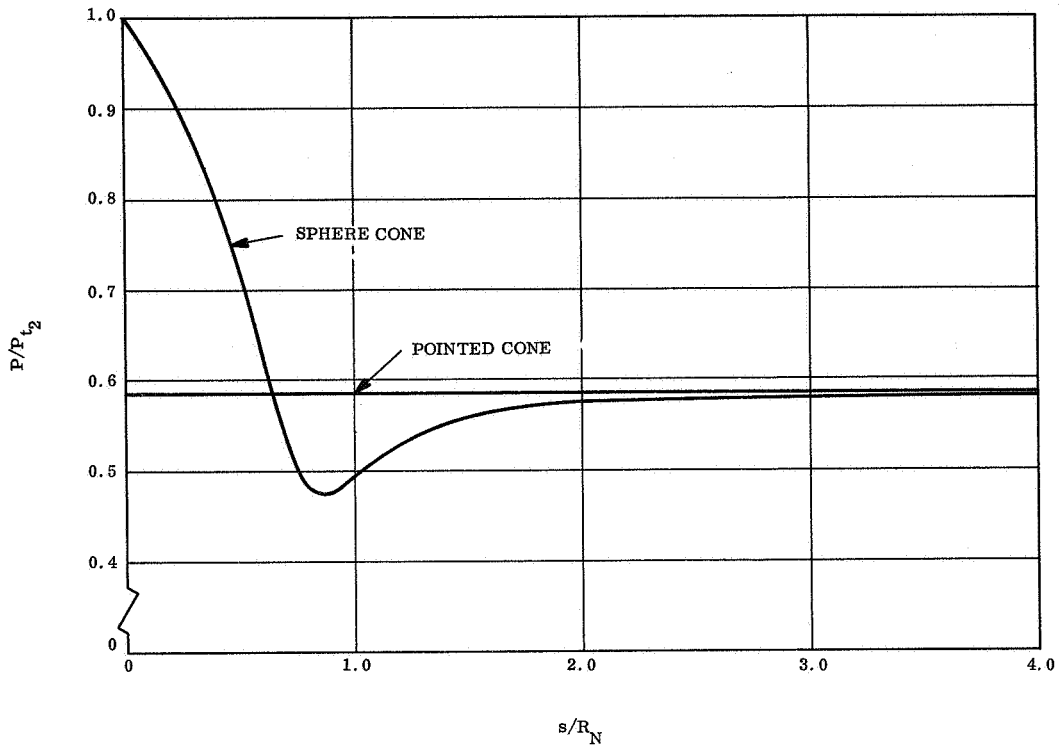

Figure 4-17. Cone Surface Pressure, (P/P_{t_2}), as a Function of s/R_N for Ideal Gas Case

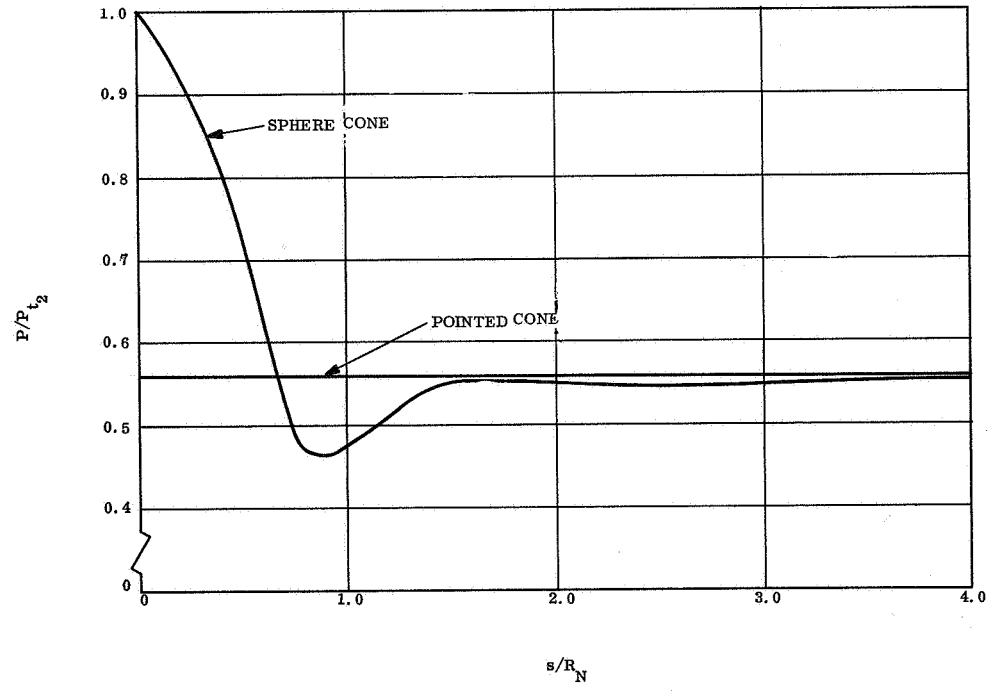

Figure 4-18. Cone Surface Pressure, (P/P_{t_2}), as a Function of s/R_N for Real Gas Case

SECTION 5
CONCLUSIONS

For a 45 degree sphere-cone, the GE Flow Field computer programs have been utilized to obtain the following numerical results:

a. Dynamic stability coefficient, $C_{M_q} + C_{M_{\dot{\alpha}}}$, as a function of R_N/R_B and x_{cg}.

b. Static stability coefficient, C_{M_α}, as a function of R_N/R_B and x_{cg}.

c. Normal force coefficient slope, C_{N_α}, as a function of R_N/R_B.

d. Normal force coefficient, $C_{N_q} + C_{N_{\dot{\alpha}}}$, as a function of R_N/R_B and x_{cg}.

e. Axial force coefficient at zero angle of attack, $(C_A)_{\alpha = 0}$, as a function of R_N/R_B.

f. Ratio of center of pressure location to cone base diameter, x_{cp}/d, as a function of R_N/R_B.

g. Bow shock wave shape and position.

h. $(1/P_{t_2})\, P_\alpha = 1/P_{t_2}\, (\partial P/\partial \alpha)_{\alpha = 0}$ as a function of s/R_N for $\phi = 0^o$, 30^o, 60^o, 90^o, where P_{t_2} is model stagnation pressure, P is model surface pressure, ϕ is azimuthal angle and s is distance measured along model surface from forward point on the axis of symmetry.

i. Cone surface pressure, (P/P_{t_2}), as a function of s/R_N.

For the real gas case, the shock layer flow downstream of the sonic line on the sphere is everywhere supersonic, and no difficulty was encountered in the computations.

For the ideal gas case, there exists a subsonic layer near the conical part of the body surface where the flow is otherwise generally supersonic. The approximation made in Section 3 enabled the completion of the computation for this case. The effect of the approximation is found to be significant for bodies of large bluntness ratios but is negligible for bodies of small bluntness ratios.

The existence of a subsonic region is found to be a direct consequence of the combination of the perfect gas assumption and the large cone angle in the study.

SECTION 6
REFERENCES

1. F.G. Gravalos, I.H. Edelfelt, and H.W. Emmons, "The Supersonic Flow About a Blunt Body of Revolution for Gases at Chemical Equilibrium," Proceedings of the 9th Annual Congress of the International Astronautical Federation, Amsterdam, 1958.

2. J.G. Logan, Jr. and C.E. Treanor, "Tables of Thermodynamic Properties of Air from 3000°K to 10,000°K at Intervals of 100°K," Cornell Aeronautical Laboratory Report No. BE-1001-A-3, January 1957.

3. J. Hilsanrath and C.W. Beckett, "Tables of Thermodynamic Properties of Argon-Free Air to 15,000°K," AEDC TN-56-12, September 1956.

4. J. Hilsanrath, C.W. Beckett, et al., "Tables of Thermal Properties of Gases," National Bureau of Standards Circular 564.

5. S.L. Stamm, "A Representation of the Thermodynamic Properties of Air in Chemical Equilibrium for Calculating Isentropic Processes," GE TIS No. R59SD415.

6. R.H. Edsall, "Tables of Thermodynamic Data for Calculating Equilibrium Air Flow Fields at Escape Velocity," GE MSD, Aerodynamic Data Memo No. 1:67.

7. H. Rie, E.A. Linkiewicz, F.D. Bosworth, "Hypersonic Dynamic Stability Final Report - Unsteady Flow Field Program," GE TIS No. 65SD367, or Air Force Aerodynamics Laboratory Report FDL-TDR-64-149 Part III, January 1967.

8. G.I. Taylor and J.W. Maccoll, "The Air Pressure on a Cone Moving at High Speed," Proceedings of the Royal Society (A), Volume 139, 1933.

9. C.H. Johnson, "The Flow Field About a Right Circular Cone at Zero Yaw," GE TIS 62SD211, November 1962.

10. E.A. Brong, "The Unsteady Flow Field About a Right Circular Cone in Unsteady Flight," GE TIS No. 66SD280, or Air Force Aerodynamic Laboratory Report FDL TDR 64-148.

11. R.S. Davis, "Analysis and Programming of a Supersonic Field with Shock Intersection," GE Report 62SD105, April 1962.

12. E.A. Brong and H. Rie, "The Supersonic Flow Field About a Body of Revolution in Unsteady Motion," GE FMTC Fundamental Memo 102, March 1963.

13. C.J. Wang, T.P. Goebel, A.B. Farnell, "Conical Flow Table," North American Aviation, Inc. Report No. NA-55-671.

APPENDIX A

NUMERICAL RESULTS IN TABULAR FORM

Table A-1. Normal Force Coefficient Slope, C_{N_α}, Static Stability Coefficient C_{M_α}, Normal Force Coefficient, $C_{N_{\dot{\alpha}}} + C_{N_q}$ and Dynamic Stability Coefficient $C_{M_{\dot{\alpha}}} + C_{N_q}$ Evaluated With Respect to Different Center of Rotation, x_{cg}/L, of a 45-Degree Cone in Ideal Gas

(A) $R_N/R_B = 1$

x_{cg}/L	C_{N_α}	C_{M_α}	$C_{N_{\dot{\alpha}}} + C_{N_q}$	$C_{M_{\dot{\alpha}}} + C_{M_q}$
0.	.90172	-.54879	.44979	-.27568
.1	.90172	-.52237	.42337	-.24721
.2	.90172	-.49595	.39696	-.22028
.3	.90172	-.46955	.37054	-.19490
.4	.90172	-.44313	.34413	-.17107
.5	.90172	-.41671	.31772	-.14879
.6	.90172	-.39028	.29130	-.12805
.7	.90172	-.36389	.26489	-.10886
.8	.90172	-.33747	.23847	-.09122
.9	.90172	-.31104	.21206	-.07512
1.0	.90172	-.28464	.13564	-.06057

Table A-1. Normal Force Coefficient Slope, C_{N_α}, Static Stability Coefficient C_{M_α}, Normal Force Coefficient, $C_{N_{\dot{\alpha}}} + C_{N_q}$ and Dynamic Stability Coefficient $C_{M_{\dot{\alpha}}} + C_{N_q}$ Evaluated With Respect to Different Center of Rotation, x_{cg}/L, of a 45-Degree Cone in Ideal Gas (Cont)

(B) $R_N/R_B = 0.75$

x_{cg}/L	C_{N_α}	C_{M_α}	$C_{N_{\dot{\alpha}}} + C_{N_q}$	$C_{M_{\dot{\alpha}}} + C_{M_q}$
0.	1.0756	-.64041	.56946	-.36853
.1	1.0756	-.60333	.53240	-.32811
.2	1.0756	-.56628	.49533	-.29024
.3	1.0756	-.52919	.45824	-.25493
.4	1.0756	-.49214	.42117	-.22218
.5	1.0756	-.45505	.38411	-.19198
.6	1.0756	-.41797	.34704	-.16433
.7	1.0756	-.38092	.30995	-.13925
.8	1.0756	-.34384	.27288	-.11671
.9	1.0756	-.30676	.23582	-.09673
1.0	1.0756	-.26969	.19875	-.07931

Table A-1. Normal Force Coefficient Slope, C_{N_α}, Static Stability Coefficient C_{M_α}, Normal Force Coefficient, $C_{N_{\dot{\alpha}}} + C_{N_q}$ and Dynamic Stability Coefficient $C_{M_{\dot{\alpha}}} + C_{N_q}$ Evaluated With Respect to Different Center of Rotation, x_{cg}/L, of a 45-Degree Cone in Ideal Gas (Cont)

(C) $R_N/R_B = 0.5$

x_{cg}/L	C_{N_α}	C_{M_α}	$C_{N_{\dot{\alpha}}} + C_{N_q}$	$C_{M_{\dot{\alpha}}} + C_{M_q}$
0.	1.0583	-.56907	.66518	-.41413
.1	1.0583	-.53046	.62660	-.37053
.2	1.0583	-.49188	.58801	-.32975
.3	1.0583	-.45331	.54943	-.29179
.4	1.0583	-.41473	.51084	-.25663
.5	1.0583	-.37612	.47225	-.22430
.6	1.0583	-.33755	.43368	-.19477
.7	1.0583	-.29896	.39508	-.16806
.8	1.0583	-.26038	.35651	-.14416
.9	1.0583	-.22179	.31791	-.12308
1.0	1.0583	-.18321	.27934	-.10480

Table A-1. Normal Force Coefficient Slope, C_{N_α}, Static Stability Coefficient C_{M_α}, Normal Force Coefficient, $C_{N_{\dot{\alpha}}} + C_{N_q}$ and Dynamic Stability Coefficient $C_{M_{\dot{\alpha}}} + C_{N_q}$ Evaluated With Respect to Different Center of Rotation, x_{cg}/L, of a 45-Degree Cone in Ideal Gas (Cont)

(D) $R_N/R_B = 0.25$

x_{cg}/L	C_{N_α}	C_{M_α}	$C_{N_{\dot{\alpha}}} + C_{N_q}$	$C_{M_{\dot{\alpha}}} + C_{M_q}$
0.	1.0246	-.62837	.80972	-.57291
.1	1.0246	-.58247	.76380	-.51051
.2	1.0246	-.53653	.71788	-.45223
.3	1.0246	-.49058	.67193	-.39806
.4	1.0246	-.44467	.62601	-.34802
.5	1.0246	-.39874	.58009	-.30208
.6	1.0246	-.35281	.53415	-.26027
.7	1.0246	-.30689	.48823	-.22258
.8	1.0246	-.26096	.44231	-.18900
.9	1.0246	-.21503	.39637	-.15953
1.0	1.0246	-.16910	.35044	-.13419

Table A-1. Normal Force Coefficient Slope, C_{N_α}, Static Stability Coefficient C_{M_α}, Normal Force Coefficient, $C_{N_{\dot{\alpha}}} + C_{N_q}$ and Dynamic Stability Coefficient $C_{M_{\dot{\alpha}}} + C_{N_q}$ Evaluated With Respect to Different Center of Rotation, x_{cg}/L, of a 45-Degree Cone in Ideal Gas (Cont)

(E) $R_N/R_B = 0$

x_{cg}/L	C_{N_α}	C_{M_α}	$C_{N_{\dot{\alpha}}} + C_{N_q}$	$C_{M_{\dot{\alpha}}} + C_{M_q}$
0.	1.0048	-.66989	.86207	-.64651
.1	1.0048	-.61965	.81182	-.57242
.2	1.0048	-.56941	.76158	-.50336
.3	1.0048	-.51917	.71134	-.43932
.4	1.0048	-.46892	.66110	-.38031
.5	1.0048	-.41868	.61086	-.32632
.6	1.0048	-.36844	.56061	-.27736
.7	1.0048	-.31820	.51038	-.23342
.8	1.0048	-.26796	.46013	-.19450
.9	1.0048	-.21771	.40989	-.16061
1.0	1.0048	-.16746	.35965	-.13174

Table A-2. Axial Force Coefficient and the Location of Center of Pressure of a 45-Degree Cone in Ideal Gas

R_N/R_B	$(C_A)\ \alpha = 0$	x_{cp}/d
1.00450	1.1944	.31671
.89614	1.1525	.29386
.79769	1.1278	.26428
.69835	1.1112	.23546
.60032	1.0999	.20763
.49895	1.0913	.18806
.39793	1.0853	.17513
.29988	1.0816	.16719
.24853	1.0804	.16501
0.	1.0800	.16667

Table A-3. The Value of $\frac{\partial P}{\partial \alpha}/P_{t_2}$ at Dimensionless Distance Measured Along Body Surface From Forward Point on Axis of Symmetry of a 45-Degree Cone in Ideal Gas

s/R_N	$\frac{\partial P}{\partial \alpha}/P_{t_2}$ [1/RAD]			
	$\phi = 0'$	$\phi = 30$	$\phi = 60$	$\phi = 90$
.84580	1.13409	.98216	.56705	0.
1.05213	1.36425	1.18148	.68213	0.
1.21168	1.50754	1.30557	.75377	0.
1.41140	1.28389	1.11189	.64195	0.
1.62961	1.28664	1.11427	.64332	0.
1.84901	1.16637	1.01011	.58319	0.
2.09930	1.10039	.95297	.55020	0.
2.32789	1.11869	.96882	.55935	0.
2.67725	1.12175	.97147	.56088	0.
2.96968	1.12749	.97644	.56375	0.
3.28417	1.12128	.97106	.56064	0.
3.81337	1.10086	.95338	.55043	0.
4.17880	1.09835	.95120	.54918	0.
4.64832	1.09952	.95222	.54976	0.
5.41086	1.09874	.95154	.54937	0.

Table A-4. Cone Surface Pressure of a 45-Degree Cone in Ideal Gas

s/R_N	P/P_{t_2}
0.	1.0
.45000	.76198
.54000	.67557
.62832	.59702
.71600	.51453
.84580	.47791
1.05213	.50882
1.21168	.52514
1.41140	.55675
1.62961	.57013
1.84901	.57706
2.09930	.57932
2.32789	.58033
2.67725	.58147
2.96968	.58281
3.28417	.58347
3.81337	.58306
4.17880	.58322
4.64832	.58343
5.41086	.58427

Table A-5. Normal Force Coefficient Slope, C_{N_α}, Static Stability Coefficient C_{M_α}, Normal Force Coefficient, $C_{N_{\dot{\alpha}}} + C_{N_q}$ and Dynamic Stability Coefficient $C_{M_{\dot{\alpha}}} + C_{N_q}$ Evaluated With Respect to Different Center of Rotation, x_{cg}/L, of a 45-Degree Cone in Real Gas

(A) $R_N/R_B = 1$

x_{cg}/L	C_{N_α}	C_{M_α}	$C_{N_{\dot{\alpha}}} + C_{N_q}$	$C_{M_{\dot{\alpha}}} + C_{M_q}$
0.	.81733	-.50204	.42008	-.25981
.1	.81733	-.47811	.39614	-.23350
.2	.81733	-.45417	.37219	-.20860
.3	.81733	-.43021	.34825	-.18509
.4	.81733	-.40628	.32431	-.16299
.5	.81733	-.38235	.30037	-.14230
.6	.81733	-.35838	.27642	-.12300
.7	.81733	-.33445	.25248	-.10511
.8	.81733	-.31052	.22854	-.08862
.9	.81733	-.28657	.20459	-.07353
1.0	.81733	-.26262	.18066	-.05985

Table A-5. Normal Force Coefficient Slope, C_{N_α}, Static Stability Coefficient C_{M_α}, Normal Force Coefficient, $C_{N_{\dot{\alpha}}} + C_{N_q}$ and Dynamic Stability Coefficient $C_{M_{\dot{\alpha}}} + C_{N_q}$ Evaluated With Respect to Different Center of Rotation, x_{cg}/L, of a 45-Degree Cone in Real Gas (Cont)

(B) $R_N/R_B = 0.75$

x_{cg}/L	C_{N_α}	C_{M_α}	$C_{N_{\dot{\alpha}}} + C_{N_q}$	$C_{M_{\dot{\alpha}}} + C_{M_q}$
0.	.97208	-.57917	.59101	-.38822
.1	.97208	-.54567	.55750	-.34904
.2	.97208	-.51216	.52400	-.31217
.3	.97208	-.47866	.49050	-.27761
.4	.97208	-.44516	.45700	-.24537
.5	.97208	-.41166	.42350	-.21543
.6	.97208	-.37816	.38998	-.18780
.7	.97208	-.34465	.35648	-.16248
.8	.97208	-.31115	.32298	-.13947
.9	.97208	-.27764	.28948	-.11877
1.0	.97208	-.24414	.25598	-.10038

Table A-5. Normal Force Coefficient Slope, C_{N_α}, Static Stability Coefficient C_{M_α}, Normal Force Coefficient, $C_{N_{\dot{\alpha}}} + C_{N_q}$ and Dynamic Stability Coefficient $C_{M_{\dot{\alpha}}} + C_{N_q}$ Evaluated With Respect to Different Center of Rotation, x_{cg}/L, of a 45-Degree Cone in Real Gas (Cont)

(C) $R_N/R_B = 0.5$

x_{cg}/L	C_{N_α}	C_{M_α}	$C_{N_{\dot{\alpha}}} + C_{N_q}$	$C_{M_{\dot{\alpha}}} + C_{M_q}$
0.	.96617	-.52389	.65950	-.41563
.1	.96617	-.48867	.63428	-.37338
.2	.96617	-.45345	.59904	-.33370
.3	.96617	-.41820	.56382	-.29659
.4	.96617	-.38298	.52860	-.26205
.5	.96617	-.34776	.49336	-.23008
.6	.96617	-.31253	.45814	-.20068
.7	.96617	-.27731	.42290	-.17386
.8	.96617	-.24208	.38768	-.14960
.9	.96617	-.20685	.35246	-.12791
1.0	.96617	-.17162	.31722	-.10879

Table A-5. Normal Force Coefficient Slope, C_{N_α}, Static Stability Coefficient C_{M_α}, Normal Force Coefficient, $C_{N_{\dot{\alpha}}} + C_{N_q}$ and Dynamic Stability Coefficient $C_{M_{\dot{\alpha}}} + C_{N_q}$ Evaluated With Respect to Different Center of Rotation, x_{cg}/L, of a 45-Degree Cone in Real Gas (Cont)

(D) $R_N/R_B = 0.25$

x_{cg}/L	C_{N_α}	C_{M_α}	$C_{N_{\dot{\alpha}}} + C_{N_q}$	$C_{M_{\dot{\alpha}}} + C_{M_q}$
0.	.98722	-.61142	.81476	-.57661
.1	.98722	-.56718	.77054	-.51465
.2	.98722	-.52294	.72630	-.45666
.3	.98722	-.47870	.68208	-.40263
.4	.98722	-.43444	.63786	-.35257
.5	.98722	-.39019	.59362	-.30648
.6	.98722	-.34594	.54940	-.26435
.7	.98722	-.30170	.50516	-.22619
.8	.98722	-.25745	.46095	-.19200
.9	.98722	-.21319	.41671	-.16177
1.0	.98722	-.16894	.37249	-.13552

Table A-5. Normal Force Coefficient Slope, C_{N_α}, Static Stability Coefficient C_{M_α}, Normal Force Coefficient, $C_{N_{\dot{\alpha}}} + C_{N_q}$ and Dynamic Stability Coefficient $C_{M_{\dot{\alpha}}} + C_{N_q}$ Evaluated With Respect to Different Center of Rotation, x_{cg}/L, of a 45-Degree Cone in Real Gas (Cont)

(E) $R_N/R_B = 0$

x_{cg}/L	C_{N_α}	C_{M_α}	$C_{N_{\dot{\alpha}}} + C_{N_q}$	$C_{M_{\dot{\alpha}}} + C_{M_q}$
0.	1.00483	-.66989	.87332	-.65499
.1	1.00483	-.61965	.82501	-.58000
.2	1.00483	-.56941	.77495	-.51000
.3	1.00483	-.51916	.72450	-.44500
.4	1.00483	-.46892	.67495	-.38600
.5	1.00483	-.41868	.62249	-.33100
.6	1.00483	-.36844	.57500	-.28100
.7	1.00483	-.31820	.52250	-.23650
.8	1.00483	-.26795	.47495	-.19700
.9	1.00483	-.21771	.42500	-.16300
1.0	1.00483	-.16747	.37500	-.13350

Table A-6. Axial Force Coefficient and the Location of Center of Pressure of a 45-Degree Cone in Real Gas

R_N/R_B	$(C_A)\ \alpha = 0$	x_{cp}/d
1.02240	1.1721	.32611
.92046	1.1395	.30642
.79132	1.1138	.26438
.71697	1.1031	.24004
.60606	1.0878	.20772
.50756	1.0755	.19380
.38231	1.0659	.18255
.36466	1.0648	.18065
.24852	1.0601	.17107
0.	1.0600	.16667

Table A-7. The Value of $\frac{\partial P}{\partial \alpha} / P_{t_2}$ at Dimensionless Distance Measured Along Body Surface from Forward Point on Axis of Symmetry of a 45-Degree Cone in Real Gas

s/R_N	$\frac{\partial P}{\partial \alpha} / P_{t_2}$ [1/RAD.]			
	$\phi = 0$	$\phi = 30$	$\phi = 60$	$\phi = 90$
.84754	.44097	.38189	.22049	0.
1.05768	1.24856	1.08129	.62428	0.
1.19184	1.46330	1.26726	.73165	0.
1.37372	1.38276	1.19751	.69138	0.
1.62956	1.07848	.93400	.53924	0.
1.79822	.93389	.80878	.46695	0.
2.03122	1.00867	.87354	.50434	0.
2.38138	1.05712	.91550	.52856	0.
2.62468	1.47926	1.28108	.73963	0.
2.95778	1.06972	.92641	.53486	0.
3.44030	1.05801	.91627	.52901	0.
3.79104	1.04182	.90225	.52091	0.
4.25914	1.04809	.90768	.52405	0.
4.91166	1.04564	.90556	.52282	0.
5.48130	1.04575	.90565	.52288	0.

Table A-8. Cone Surface Pressure of a 45-Degree Cone in Real Gas

s/R_N	P/P_{t_2}
0.	1.0
.45400	.77042
.54000	.68482
.62832	.59727
.71600	.51750
.84754	.46068
1.05768	.48897
1.19184	.50957
1.37372	.54084
1.62956	.55171
1.79822	.55135
2.03122	.54753
2.38138	.54776
2.62468	.54852
2.95778	.55054
3.44030	.55203
3.79104	.55195
4.25914	.55217
4.91166	.55272
5.48130	.55246